RESEARCH ARTICLE

DIAGNOSTIC OF A LASER-INDUCED OPTICAL BREAKDOWN BASED ON HALF-WIDTH AT HALF AREA OF H_α, H_β, AND H_γ LINES

CHRISTIAN G. PARIGGER*

The University of Tennessee Space Institute, Center for Laser Applications, 411 B.H. Goethert Parkway,
Tullahoma, Tennessee-37388, USA.

Abstract: Measurements and analysis of broadened profiles of the H-alpha, H-beta, and H-gamma lines following laser-induced optical breakdown are presented. Laser induced optical breakdown (LIOB) is generated by focusing Nd:YAG laser radiation into a pulsed methane flow. The inferred electron densities Ne are typically in the range of 0.5 to 5×10^{17} cm^{-3} for time delays of 2.1 to 0.4 µs after optical breakdown. In this paper we focus on comparing N_e determination using Full-width-half-area (FWHA) versus use of Full-width-half-maximum (FWHM). We found that for measurements of N_e in the order of 10^{17} cm^{-3} and higher, the usage of FWHM is preferred. We also allowed for the asymmetry of theoretical H-beta profiles while fitting the experimental profiles.

PACS: 52.50. Jm, 52.25. Os, 32.70. Jz, 33.70. Jg, 32.30.-r, 32.20.-t.

1. INTRODUCTION

Plasmas formed by a Laser-Induced Optical Breakdown (LIOB) in gases can be diagnosed using the Stark broadening of hydrogen lines. In our work, typical laser-induced plasma characteristics comprise electron density up to 10^{19} cm^{-3} and excitation temperatures of 10^5 K, or approximately 10 eV. Usually we use 10-nanosecond, 100 milliJoule/pulse laser radiation focused in gaseous samples. Application of time-resolved atomic spectroscopy allows us to measure electron density and temperature during the plasma decay. For a time delay of 5 nano-second and a gate width of 2 nanosecond, we measured for H-alpha the significant line-width of 25.4 ± 3.5 nm and red shift of 2.7 ± 0.6 nm. The H-beta profile for a time-delay of 100 ns with a 6-ns gate was measured to be 17.8 ± 2.5 nm. In papers [1, 2], the LIOB was studied in gaseous hydrogen and the plasmas were diagnosed using H-alpha line in [1] and H-beta line in [2].

In our papers [3, 4], the LIOB was studied in a pulsed methane flow; the plasma was diagnosed using time-resolved measurements of profiles of H-alpha, H-beta, and H-gamma-lines. In [3] the electron density was deduced from the Stark broadening of only H-alpha and H-beta lines, while the measured widths of the H-gamma line have not been analyzed. In [4], we analyzed the widths of the H-gamma line measured in [3]. For 18 instants of time in the range between 0.4 – 2.1 µs after the LIOB and for 2 different gas pressures, we deduced the electron density N_e from the Stark broadening of the H-gamma line and compared the results with the corresponding values of N_e obtained from the H-alpha and H-beta lines.

In the present paper we analyze the same H-alpha, H-beta, and H-gamma spectral profiles using an alternative technique based on Full-width at half area (FWHA). Then we compare the outcome with the corresponding results obtained from Full-width at half maximum (FWHM).

2. EXPERIMENTAL DETAILS

The time-resolved measurements of LIOB comprised typical experimental arrangements for laser-induced breakdown spectroscopy (LIBS): nominal nanosecond Q-switched laser (8-ns, 75-mJ per pulse infrared 1064-nm radiation from a model Continuum YG680-10 Nd:YAG laser), spectrometer (1/2 m model 500 SpectraPro Acton Research Corporation) and intensified linear diode array

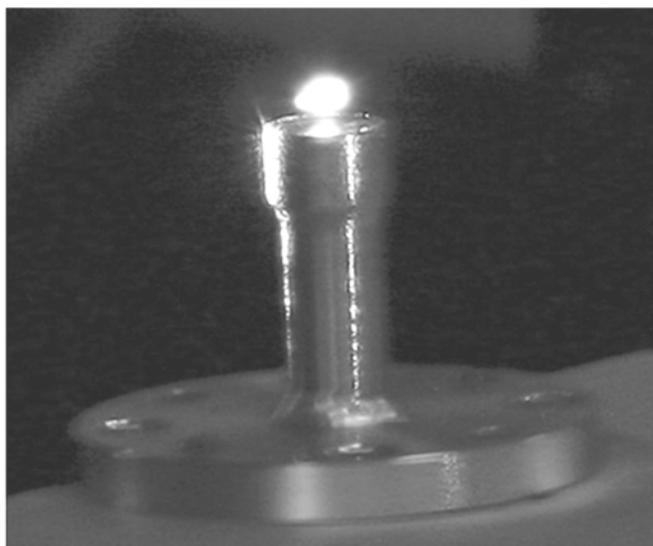* Corresponding Author: *cparigge@tennessee.edu.*

Fig. 1: Laser-Induced Optical Breakdown (LIOB) above nozzle used for expanding Methane flow
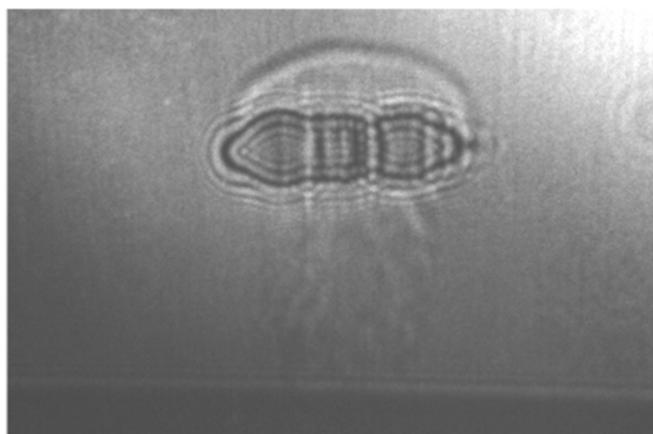

Fig. 2: Schadowgraph of LIOB in expanding Methane flow

(model 1460 Princeton Applied Research detector/controller optical multichannel analyzer). The captured time-resolved data, averaged over 100 individual LIOB events, were detector-noise/back-ground corrected, wavelength and detector sensitivity calibrated. Figure 1 illustrates the nozzle that we used, and Fig. 2 shows a typical shadowgraph of LIOB in the expanding flow. Further details of the experimental procedures are summarized in [3].

Individual profiles of the Balmer series lines H-alpha, H-beta, and H-gamma, were measured subsequent to optical breakdown. Comparison of the recorded intensities of these lines allows one, in principle, to infer electron temperature, T_e, provided reasonable complete profiles are recorded. Typical for our LIOB measurements

however are incomplete H-beta and H-gamma line profiles due to significant contribution of background radiation early in the methane breakdown, high electron density, N_e, early in the plasma decay followed by occurrence of molecular spectra that overlap Balmer series lines, particularly from C_2.

Temperature estimates are inferred by using the relative signal-strengths of the three line profiles H-alpha, H-beta, and H-gamma, although several errors in determining T_e are noted. For example, determination of background radiation at a particular time delay from LIOB, or application of sensitivity and wavelength calibrations, or comparison of line-profiles from separate 100-event averages recorded for only one particular Balmer line at a time.

The results for the inferred T_e are in the 10,000 K (time delay 2.1 µs) to 20,000 K (time delay of 0.4 µs) range, using the area of the incomplete H-beta and H-gamma lines and the area of the H-alpha line in constructing Boltzmann plots, analogous as discussed in [1]. For both gas pressures of 2.7×10^5 Pa and 6.5×10^5 Pa, almost identical results are found for T_e. When extending the curve fitting beyond the measured spectral windows used for the three lines, and using the area of these extended profiles, typically 50% higher T_e is found: these temperatures constitute an upper limit of 15,000 K and 30,000 K for time delays of 2.1 µs and 0.4 µs, respectively, with similar results obtained for both pressures. Figure 3 illustrates the inferred temperatures for the two pressures. Indicated here are the results for
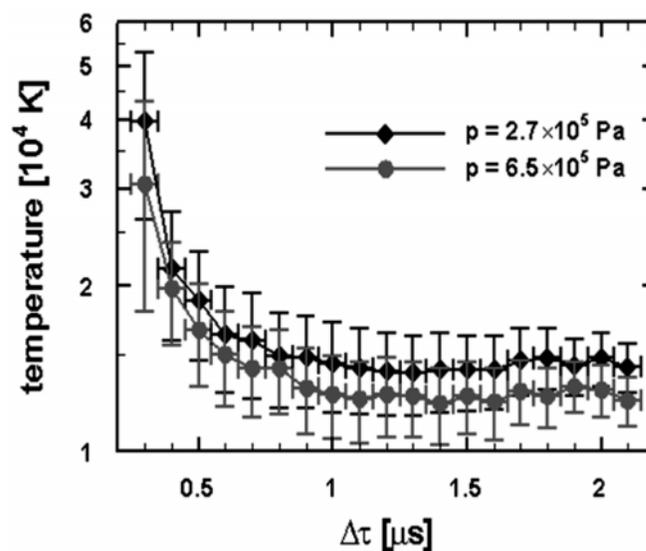

Fig. 3: Inferred temperatures from the Balmer Series H-alpha, H-beta, and H-gamma lines

0.3 microseconds delay that also show relatively large error bars.

Tables 1–3 show measured FWHM of the H-alpha, H-beta, and H-gamma lines, respectively, for two different gas pressures: 2.7×10^5 Pa and 6.5×10^5 Pa. The data are presented in tabular form for different time delays, t_{delay}, from LIOB. The experimental error bars indicate the estimated total error of determining the FWHM line widths for the Balmer series lines.

Table 1: Measured H-alpha FWHM Widths

t_{delay} [μs]	2.7×10^5 Pa: width [nm]	6.5×10^5 Pa: width [nm]
0.4	2.8 ± 0.3	2.7 ± 0.3
0.5	2.4 ± 0.3	2.3 ± 0.3
0.6	2.1 ± 0.3	2.1 ± 0.3
0.7	1.9 ± 0.2	1.9 ± 0.2
0.8	1.7 ± 0.2	1.7 ± 0.2
0.9	1.6 ± 0.2	1.5 ± 0.2
1.0	1.4 ± 0.2	1.4 ± 0.2
1.1	1.3 ± 0.2	1.3 ± 0.2
1.2	1.2 ± 0.1	1.2 ± 0.2
1.3	1.1 ± 0.1	1.1 ± 0.1
1.4	1.0 ± 0.1	1.0 ± 0.1
1.5	1.0 ± 0.1	0.92 ± 0.1
1.6	0.89 ± 0.1	0.87 ± 0.1
1.7	0.86 ± 0.1	0.78 ± 0.1
1.8	0.79 ± 0.1	0.77 ± 0.1
1.9	0.77 ± 0.1	0.69 ± 0.1
2.0	0.73 ± 0.1	0.67 ± 0.1
2.1	0.70 ± 0.1	0.61 ± 0.1

Table 2: Measured H-beta FWHM Widths

t_{delay} [μs]	2.7×10^5 Pa: width [nm]	6.5×10^5 Pa: width [nm]
0.4	10.0 ± 0.9	10.0 ± 0.5
0.5	9.0 ± 0.8	8.7 ± 0.5
0.6	8.1 ± 0.7	7.8 ± 0.5
0.7	7.4 ± 0.5	7.3 ± 0.4
0.8	6.8 ± 0.4	6.5 ± 0.4
0.9	6.3 ± 0.4	5.9 ± 0.4
1.0	5.9 ± 0.4	5.4 ± 0.4
1.1	5.3 ± 0.4	5.1 ± 0.3
1.2	5.0 ± 0.3	4.8 ± 0.3
1.3	4.7 ± 0.3	4.5 ± 0.3
1.4	4.4 ± 0.3	4.1 ± 0.3
1.5	4.1 ± 0.3	3.9 ± 0.3
1.6	3.9 ± 0.3	3.7 ± 0.2
1.7	3.8 ± 0.3	3.5 ± 0.2
1.8	3.6 ± 0.2	3.3 ± 0.2
1.9	3.3 ± 0.2	3.1 ± 0.2
2.0	3.1 ± 0.2	2.9 ± 0.2
2.1	2.9 ± 0.2	2.8 ± 0.2

Table 3: Measured H-gamma FWHM Widths

t_{delay} [μs]	2.7×10^5 Pa: width [nm]	6.5×10^5 Pa: width [nm]
0.4	11.0 ± 2.0	10.4 ± 2.0
0.5	10.7 ± 2.0	9.5 ± 2.0
0.6	8.7 ± 1.5	8.6 ± 1.5
0.7	8.1 ± 1.5	7.8 ± 1.5
0.8	7.6 ± 1.5	6.7 ± 1.5
0.9	6.7 ± 1.5	6.3 ± 1.5
1.0	6.2 ± 1.5	6.2 ± 1.5
1.1	6.0 ± 1.0	5.8 ± 1.0
1.2	5.8 ± 1.0	5.5 ± 1.0
1.3	5.6 ± 1.0	5.4 ± 1.0
1.4	5.3 ± 1.0	5.1 ± 1.0
1.5	5.2 ± 1.0	5.1 ± 1.0
1.6	5.0 ± 1.0	4.7 ± 1.0
1.7	5.0 ± 1.0	5.0 ± 1.0
1.8	5.0 ± 1.0	4.6 ± 1.0
1.9	5.0 ± 1.0	4.4 ± 1.0
2.0	4.7 ± 1.0	3.6 ± 1.0
2.1	4.6 ± 1.0	3.6 ± 1.0

Tables 4–6 show measured FWHA of the H-alpha, H-beta, and H-gamma lines, respectively, for two different gas pressures: 2.7×10^5 Pa and 6.5×10^5 Pa. The data are presented in tabular form for different time delays, tdelay, from LIOB. The experimental error bars indicate the estimated total error of determining the FWHA line widths for the Balmer series lines.

Table 4: Measured H-alpha FWHA Widths

t_{delay} [μs]	2.7×10^5 Pa: width [nm]	6.5×10^5 Pa: width [nm]
0.4	2.02 ± 0.40	2.00 ± 0.40
0.5	1.81 ± 0.36	1.81 ± 0.36
0.6	1.65 ± 0.33	1.65 ± 0.33
0.7	1.53 ± 0.31	1.52 ± 0.30
0.8	1.42 ± 0.28	1.41 ± 0.28
0.9	1.33 ± 0.27	1.32 ± 0.26
1.0	1.24 ± 0.25	1.23 ± 0.25
1.1	1.17 ± 0.23	1.16 ± 0.23
1.2	1.11 ± 0.22	1.09 ± 0.22
1.3	1.04 ± 0.21	1.04 ± 0.21
1.4	0.99 ± 0.20	0.99 ± 0.20
1.5	0.94 ± 0.19	0.88 ± 0.18
1.6	0.89 ± 0.18	0.89 ± 0.18
1.7	0.85 ± 0.17	0.87 ± 0.17
1.8	0.82 ± 0.16	0.83 ± 0.17
1.9	0.79 ± 0.16	0.80 ± 0.16
2.0	0.77 ± 0.15	0.79 ± 0.16
2.1	0.76 ± 0.15	0.77 ± 0.15

Table 5: Measured H-beta FWHA Widths

t_{delay} [μs]	2.7×10^5 Pa: width [nm]	6.5×10^5 Pa: width [nm]
0.4	5.18 ± 1.04	5.14 ± 1.03
0.5	4.90 ± 0.98	4.86 ± 0.97
0.6	4.59 ± 0.92	4.56 ± 0.91
0.7	4.34 ± 0.87	4.28 ± 0.86
0.8	4.11 ± 0.82	4.02 ± 0.80
0.9	3.90 ± 0.78	3.79 ± 0.76
1.0	3.69 ± 0.74	3.56 ± 0.71
1.1	3.49 ± 0.70	3.38 ± 0.68
1.2	3.31 ± 0.66	3.20 ± 0.64
1.3	3.16 ± 0.63	3.06 ± 0.61
1.4	3.02 ± 0.60	2.94 ± 0.59
1.5	2.88 ± 0.58	2.83 ± 0.57
1.6	2.76 ± 0.55	2.73 ± 0.55
1.7	2.66 ± 0.53	2.64 ± 0.53
1.8	2.55 ± 0.51	2.59 ± 0.52
1.9	2.45 ± 0.49	2.60 ± 0.52
2.0	2.35 ± 0.47	2.63 ± 0.53
2.1	2.27 ± 0.45	2.64 ± 0.53

Table 6: Measured H-gamma FWHA Widths

t_{delay} [μs]	2.7×10^5 Pa: width [nm]	6.5×10^5 Pa: width [nm]
0.4	5.66 ± 1.13	5.64 ± 1.13
0.5	5.67 ± 1.13	5.44 ± 1.09
0.6	5.27 ± 1.05	5.23 ± 1.05
0.7	5.11 ± 1.02	5.04 ± 1.01
0.8	4.93 ± 0.99	4.84 ± 0.97
0.9	4.77 ± 0.95	4.67 ± 0.93
1.0	4.60 ± 0.92	4.49 ± 0.90
1.1	4.46 ± 0.89	4.33 ± 0.87
1.2	4.32 ± 0.86	4.20 ± 0.84
1.3	4.20 ± 0.84	4.10 ± 0.82
1.4	4.09 ± 0.82	3.99 ± 0.80
1.5	3.98 ± 0.80	3.92 ± 0.78
1.6	3.93 ± 0.79	3.88 ± 0.78
1.7	3.88 ± 0.78	3.96 ± 1.19
1.8	3.83 ± 0.77	3.94 ± 1.18
1.9	3.81 ± 1.14	4.00 ± 1.20
2.0	3.79 ± 1.14	4.01 ± 1.20
2.1	3.81 ± 1.14	4.08 ± 1.22

3. ANALYSIS

The combined contribution to the FWHM of the instrumental and Doppler broadening (as well as of the fine structure) is negligibly small compared to the measured widths. For example, for the H-gamma line those combined contributions do not exceed 0.14 nm for t_{delay} = 0.4 µs, when the experimental FWHM is at least 10.4 nm, and do not exceed 0.11 nm for t_{delay} = 2.1 µs, when the experimental FWHM is at least 3.6 nm. A similar situation is for the H-beta and H-alpha lines — except for few largest time delays for the H-alpha line, where those contributions reach up to about 15% of the measured FWHM and should be taken into account.

For each of these three hydrogen lines, for 18 time delays and 2 different gas pressures the values of the electron density N_e were deduced in paper [4] based on the Stark broadening tables and analytical results from [5, 6]. Table 7 shows the values of N_e deduced from these three hydrogen lines for the pressure 2.7×10^5 Pa; Table 8 shows the values of N_e deduced from these three hydrogen lines for the pressure 6.5×10^5 Pa.

Table 7: Deduced N_e from FWHM for Pressure of 2.7×10^5 Pa

t_{delay} [µs]	H_α N_e [10^{17} cm^{-3}]	H_β N_e [10^{17} cm^{-3}]	H_γ Ne [10^{17} cm^{-3}]
0.4	5.0 ± 0.4	2.9 ± 0.8	2.6 ± 0.7
0.5	3.8 ± 0.4	2.5 ± 0.7	2.5 ± 0.7
0.6	3.0 ± 0.4	2.2 ± 0.6	1.9 ± 0.5
0.7	2.5 ± 0.4	1.9 ± 0.5	1.7 ± 0.5
0.8	2.1 ± 0.3	1.6 ± 0.4	1.5 ± 0.5
0.9	1.9 ± 0.3	1.4 ± 0.4	1.3 ± 0.4
1.0	1.6 ± 0.3	1.3 ± 0.4	1.2 ± 0.4
1.1	1.4 ± 0.2	1.2 ± 0.3	1.1 ± 0.25
1.2	1.3 ± 0.2	1.1 ± 0.3	1.05 ± 0.25
1.3	1.15 ± 0.2	1.0 ± 0.3	1.0 ± 0.28
1.4	1.0 ± 0.2	0.87 ± 0.3	0.95 ± 0.28
1.5	1.0 ± 0.2	0.79 ± 0.3	0.92 ± 0.28
1.6	0.90 ± 0.2	0.76 ± 0.2	0.90 ± 0.28
1.7	0.84 ± 0.1	0.75 ± 0.2	0.90 ± 0.29
1.8	0.72 ± 0.1	0.68 ± 0.2	0.90 ± 0.29
1.9	0.69 ± 0.1	0.60 ± 0.2	0.90 ± 0.29
2.0	0.63 ± 0.1	0.55 ± 0.2	0.80 ± 0.30
2.1	0.58 ± 0.1	0.50 ± 0.2	0.77 ± 0.29

Table 8: Deduced N_e from FWHM for Pressure of 6.5×10^5 Pa

t_{delay} [µs]	H_α N_e [10^{17} cm^{-3}]	H_β N_e [10^{17} cm^{-3}]	H_γ N_e [10^{17} cm^{-3}]
0.4	4.9 ± 0.8	2.9 ± 0.8	2.4 ± 0.7
0.5	3.6 ± 0.7	2.4 ± 0.7	2.2 ± 0.6
0.6	3.0 ± 0.6	2.1 ± 0.6	1.8 ± 0.5
0.7	2.5 ± 0.5	1.8 ± 0.5	1.6 ± 0.5
0.8	2.1 ± 0.4	1.5 ± 0.4	1.3 ± 0.4
0.9	1.75 ± 0.4	1.3 ± 0.4	1.2 ± 0.4
1.0	1.6 ± 0.4	1.2 ± 0.4	1.2 ± 0.4
1.1	1.4 ± 0.3	1.1 ± 0.3	1.05 ± 0.25
1.2	1.3 ± 0.3	1.0 ± 0.3	1.0 ± 0.26
1.3	1.15 ± 0.3	0.92 ± 0.3	1.0 ± 0.28
1.4	1.0 ± 0.3	0.79 ± 0.3	0.91 ± 0.28
1.5	0.92 ± 0.3	0.76 ± 0.3	0.91 ± 0.28
1.6	0.86 ± 0.3	0.72 ± 0.3	0.78 ± 0.27
1.7	0.70 ± 0.3	0.66 ± 0.3	0.90 ± 0.29
1.8	0.69 ± 0.3	0.60 ± 0.3	0.77 ± 0.28
1.9	0.57 ± 0.3	0.55 ± 0.3	0.71 ± 0.28
2.0	0.55 ± 0.4	0.50 ± 0.4	0.51 ± 0.25
2.1	0.46 ± 0.4	0.48 ± 0.4	0.51 ± 0.25

In the present paper the analysis of the FWHA profiles is accomplished with computed profiles presented by Gigosos et al. [7]. Tables 9 and 10 show the results when using the provided diagnosis maps [7]. In comparison with the FWHM Tables 7 and 8, inferred electron densities from the FWHA widths are smaller by a factor of two for early time delays, or for electron densities $> 10^{17}$ cm^{-3}. For electron densities $< 10^{17}$ cm^{-3}, both methods yield reasonable agreement. Reasons for the disparities at higher electron densities are the incompletely resolved line profiles for H-alpha, H-beta, and H-gamma. However, for measurements of N_e in the order of 10^{17} cm^{-3} the usage of FWHM from [5, 6] is preferred (see Ref. [8] and Tables 8 and 9 of the present paper).

The error bars of the deduced N_e are due to several factors as follows. The primary factor is the error bars of the experimental widths. There are two secondary factors: The uncertainty in the temperature and the uncertainty in the reduced mass of the pairs "perturber-radiator". Speaking of the latter: since the discharge occurs in methane (CH_4), the perturbers could be not only hydrogen ions (protons), but also carbon ions. The reduced mass is µ = 0.5 for the pairs H-H$^+$ or µ = 0.923 for the pairs H-C$^+$ and H-C^{++}.

Table 9: Deduced N_e from FWHA for Pressure of 2.7×10^5 Pa

t_{delay} [μs]	H_α N_e [$10^{17} cm^{-3}$]	H_β N_e [$10^{17} cm^{-3}$]	H_γ N_e [$10^{17} cm^{-3}$]
0.4	2.47 ± 0.60	1.11 ± 0.25	1.26 ± 0.42
0.5	2.18 ± 0.56	1.04 ± 0.25	1.27 ± 0.42
0.6	1.92 ± 0.57	0.96 ± 0.24	1.12 ± 0.36
0.7	1.69 ± 0.56	0.89 ± 0.24	1.07 ± 0.34
0.8	1.49 ± 0.53	0.83 ± 0.23	1.01 ± 0.31
0.9	1.32 ± 0.48	0.76 ± 0.22	0.96 ± 0.29
1.0	1.17 ± 0.42	0.71 ± 0.21	0.91 ± 0.26
1.1	1.05 ± 0.37	0.65 ± 0.20	0.87 ± 0.24
1.2	0.95 ± 0.32	0.60 ± 0.18	0.84 ± 0.23
1.3	0.86 ± 0.27	0.56 ± 0.17	0.80 ± 0.21
1.4	0.79 ± 0.24	0.52 ± 0.16	0.78 ± 0.20
1.5	0.74 ± 0.22	0.48 ± 0.15	0.75 ± 0.19
1.6	0.68 ± 0.19	0.45 ± 0.14	0.74 ± 0.19
1.7	0.64 ± 0.18	0.43 ± 0.13	0.73 ± 0.19
1.8	0.61 ± 0.17	0.40 ± 0.12	0.72 ± 0.18
1.9	0.58 ± 0.16	0.37 ± 0.12	0.71 ± 0.27
2.0	0.56 ± 0.15	0.35 ± 0.11	0.71 ± 0.27
2.1	0.55 ± 0.15	0.33 ± 0.10	0.71 ± 0.27

Table 10: Deduced N_e from FWHA for pressure of 6.5×10^5 Pa

t_{delay} [μs]	H_α N_e [$10^{17} cm^{-3}$]	H_β N_e [$10^{17} cm^{-3}$]	H_γ N_e [$10^{17} cm^{-3}$]
0.4	2.45 ± 0.59	1.10 ± 0.25	1.25 ± 0.41
0.5	2.17 ± 0.56	1.03 ± 0.25	1.18 ± 0.39
0.6	1.92 ± 0.57	0.95 ± 0.24	1.11 ± 0.36
0.7	1.68 ± 0.56	0.87 ± 0.24	1.04 ± 0.33
0.8	1.47 ± 0.52	0.80 ± 0.23	0.98 ± 0.30
0.9	1.30 ± 0.47	0.73 ± 0.22	0.93 ± 0.27
1.0	1.15 ± 0.41	0.67 ± 0.20	0.88 ± 0.25
1.1	1.03 ± 0.36	0.62 ± 0.19	0.84 ± 0.23
1.2	0.93 ± 0.31	0.57 ± 0.18	0.80 ± 0.21
1.3	0.85 ± 0.27	0.53 ± 0.16	0.78 ± 0.20
1.4	0.79 ± 0.24	0.50 ± 0.15	0.75 ± 0.19
1.5	0.67 ± 0.19	0.47 ± 0.15	0.74 ± 0.19
1.6	0.68 ± 0.19	0.44 ± 0.14	0.73 ± 0.19
1.7	0.66 ± 0.18	0.42 ± 0.13	0.74 ± 0.29
1.8	0.62 ± 0.17	0.41 ± 0.13	0.74 ± 0.29
1.9	0.59 ± 0.16	0.41 ± 0.13	0.75 ± 0.29
2.0	0.58 ± 0.16	0.42 ± 0.13	0.76 ± 0.30
2.1	0.56 ± 0.15	0.42 ± 0.13	0.77 ± 0.31

In addition to use of tables discussed above, experimental results presented in [3] are also evaluated using the published program [9] for H-beta fitting. Figure 4 shows results when using a quite old Vidal-Cooper-Smith (VCS) model (reproduced in [9]), Fig. 5 shows results when using a relatively new computational model [9] with the reduced
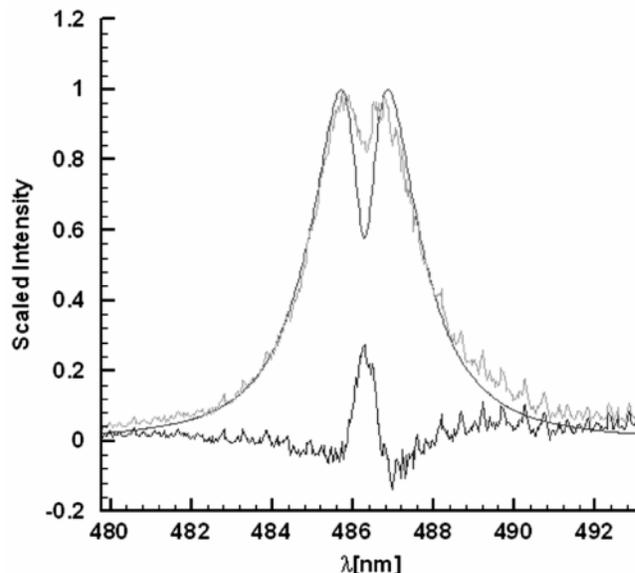

Fig. 4: Experimental H-beta line profile fitted with VCS model (reproduced in [9]), center wavelength = 486.284 nm, N_e = 0.578 × 10^{17} cm^{-3}. Center Dip (%) = 42.2% and FWHM = 3.086 nm. Experimental profile corresponds to the pressure 2.7 × 10^5 Pa and to the time delay 2.1 µs. The bottom curve is the difference between the experimental profile and the VCS profile
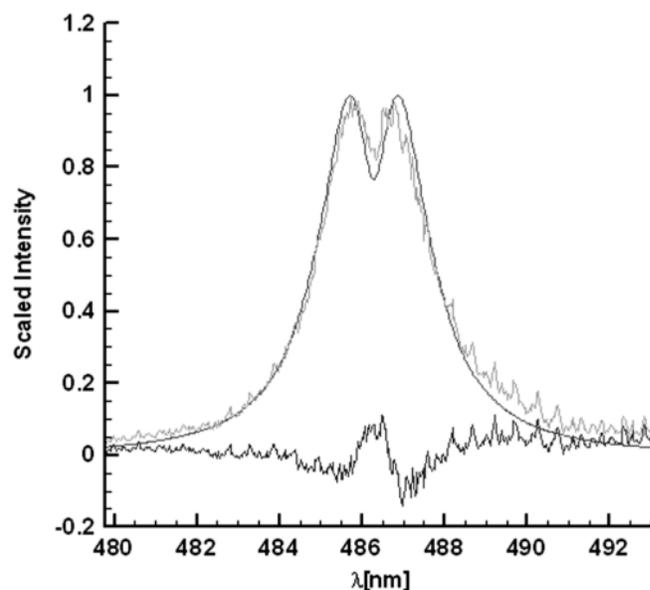

Fig. 5: Experimental H-beta line profile fitted with the computation model from [9], center wavelength = 486.284 nm, N_e = 0.585 × 10^{17} cm^{-3}

mass $\mu = 1$. Clearly, better results are obtained by fitting with the computational model rather than with VCS model (see Fig. 5). Figures 4 and 5 show experi-mental data [3] and fitting results for the lower of the two pressures at 2.1 µs time delay. The figures also show the previously debated overlap from C$_2$ molecular spectra [3], i.e., see in Figs 4 and/or 5 the peaks of 3% to 8% of the maximum that are clearly discernable in the difference curve (residual) in the region of 488-nm to 491-nm.

Recently published theoretical work and analyses of the asymmetry of the H-beta profile [10, 11] allow us to further improve the fitted profiles. Figures 6 and 7 illustrate these results for a time delay of 0.9 µs. Noteworthy is slight presence of carbon molecular spectra [3] of the C$_2$ Swan band emission indicated by small peaks in the difference spectrum, e.g., see bottom curve of Fig. 7. Presence of molecular recombination spectra subsequent and/or concurrent with atomic spectra is quite typical [12 – 14] in time-resolved laser-induced break-down spectroscopy.

It is instructive to compare the density $N_e = 0.585 \times 10^{17}$ cm^{-3} deduced by fitting the experimental profile from Fig. 5 performed by using the computation model [7] with the density $N_e = (0.50 \pm 0.2) \times 10^{17}$ cm^{-3} obtained by employing FWHM from [5, 6] (see above Table 7, the last row, 3rd column) and with the density $N_e = (0.33 \pm 0.10) \times 10^{17}$ cm^{-3} obtained by utilizing FWHA from [7] (see above Table 9, the last row, 3rd column). It is seen

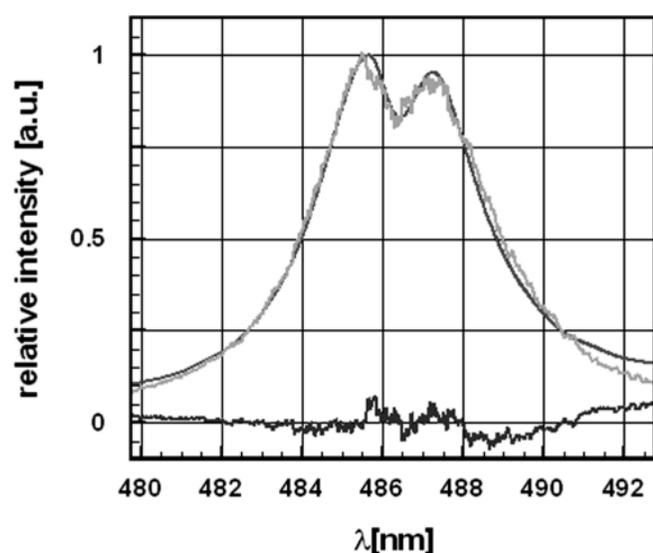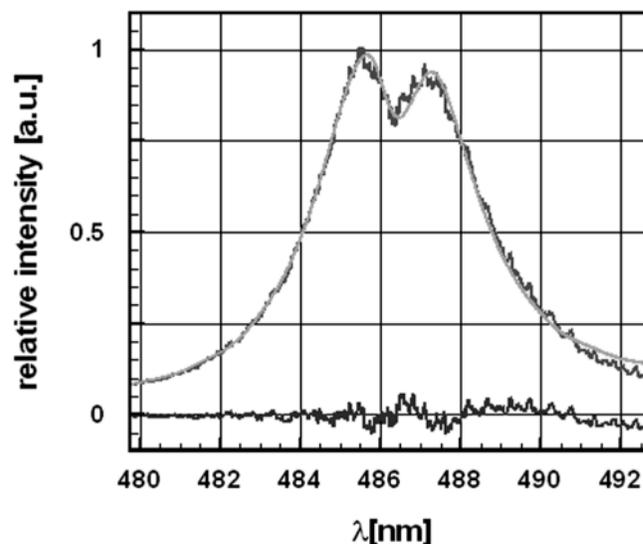**Fig. 7:** Measured and fitted H-beta profile, using asymmetric H-beta line shapes [10, 11] for $T = 10,000$ K and $N_e = 1.0 \times 10^{17}$ cm^{-3}. Experimental profile corresponds to the pressure 6.5×10^5 Pa and to the time delay 0.9 µs

that the density obtained by employing FWHM from [5, 6] is in a good agreement with the density obtained by fitting the profile with the computational model [11], while the density obtained by utilizing FWHA from [7] is in disagreement by a factor of two. Thus, the employment of FWHM from [5, 6] is a quite reliable tool for deducing the density, which is of course simpler than fitting the entire experimental profile.

4. CONCLUSIONS

We had previously demonstrated that time-resolved measurements of profiles of H-alpha, H-beta, and H-gamma lines provide good diagnostics for the LIOB in methane. The electron densities N_e deduced from the H-gamma and H-beta lines had shown generally a good agreement with each other. Slightly higher values of the electron density, deduced from the H-alpha line at some time delays, were probably due to a self-absorption in this line.

In the present paper we focused on comparing N_e determination using Full-width-half-area (FWHA) versus use of Full-width-half-maximum (FWHM). We found that for measurements of N_e in the order of 10^{17} cm^{-3} and higher, the usage of FWHM is preferred. We also allowed for the asymmetry of theoretical H-beta profiles while fitting the experimental profiles and found that this further improves the accuracy of the determination of the electron density N_e.

Fig. 6: Measured and fitted H-beta profile, using asymmetric H-beta line shapes [10, 11] for $T = 10,000$ K and $N_e = 1.0 \times 10^{17}$ cm^{-3}. Experimental profile corresponds to the pressure 2.7×10^5 Pa and to the time delay 0.9 µs

REFERENCES

[1] C.G. Parigger, D.H. Plemmons, and J.W.L. Lewis, *Appl. Optics.*, **34**, (1995), 3325.

[2] C.G. Parigger, D.H. Plemmons, and E. Oks, *Appl. Optics.*, **42**, (2003), 5992.

[3] C.G. Parigger, M. Dackman, and J.O. Hornkohl, *Appl. Optics.*, **47**, (2008), G1.

[4] C.G. Parigger and E. Oks, *International Review of Atomic and Molecular Physics*, **1**, 13 (2010).

[5] E. Oks, "Stark Broadening of Hydrogen and Hydrogenlike Spectral Lines in Plasmas: The Physical Insight", *Alpha Science International*, Oxford, 2006.

[6] E. Oks, *in Proc. 18th Intern. Conf. Spectral Line Shapes, AIP Conf. Proceedings 874*, *American Institute of Physics*, New York, 2006, pp. 19.

[7] M.A. Gigosos, M.Á. González, and V. Cardeñoso, *Spectrochim. Acta B*, (2003), 1489.

[8] C. Parigger and E. Oks, *Intern. J. Spectroscopy.*, **2010**, (2010), Article ID 936385.

[9] R.Zîkić, M.A. Gigosos, M. Ivković, M.Á. González, N. Konjević, *Spectrochim. Acta B*, (2002), 987.

[10] S. Djurović, M. Ćirišan, A.V. Demura, G.V. Demchenko, D. Nikolić, M.A. Gigosos, and M.Á. González, *Phys. Rev. E*, **79**, (2009), 046402.

[11] M.Á. González, *Prívate Communication*, (2009).

[12] C. Parigger, "Laser-induced Breakdown in Gases: Experiments and Simulation", Chapter 4 in A.W. Miziolex, V. Palleschi, I. Schechter eds. *Laser Induced Breakdown Spectroscopy*, Cambridge University Press, New York 2006.

[13] C.G. Parigger, James. O. Hornkohl, and L. Nemes, *Intern. J. Spectroscopy*, **2010**, (2010), Article ID 593820.

[14] C.G. Parigger and J. Hornkohl, *International Review of Atomic and Molecular Physics*, **1**, 26, (2010).

[15] E. Oks, "Plasma Spectroscopy: The Influence of Microwave and Laser Fields", *Springer Series on Atoms and Plasmas*, **9**, Springer, New York, 1995.

[16] H.R. Griem, *Spectral Line Broadening by Plasmas*, Academic, New York, 1964.